**ESKİŞEHİR TEKNİK ÜNİVERSİTESİ BİLİM VE TEKNOLOJİ DERGİSİ B- TEORİK BİLİMLER**

Eskişehir Technical University Journal of Science and Technology B- Theoritical Sciences

**2018, 6(2), pp. 219 - 227, DOI: 10.20290/aubtdb.463901**

# SINGLE LAYER $ReS_2H_2$ : STABILITY, RAMAN ACTIVITY AND ELECTRONIC PROPERTIES

**Elif ÜNSAL[1], Hasan ŞAHİN [2, 3, *]**

[1] Department of Physics, Faculty of Science, İzmir Institute of Technology, İzmir, Turkey
[2] Department of Photonics, Faculty of Science, İzmir Institute of Technology, İzmir, Turkey
[3] ICTP-ECAR, Eurasian Center for Advanced Research, İzmir Institute of Technology, İzmir, Turkey

## ABSTRACT

In this study, the structural, vibrational and electronic properties of the hydrogenated single layer of $ReS_2$ are investigated by performing the first principle calculations based on density functional theory. We found that the characteristic properties of the monolayer $ReS_2$ can be manipulated upon the hydrogen functionalization. As the monolayer $ReS_2$, the $ReS_2H_2$ has distorted 1T phase; however, the bonding in Re slab significantly varies with the hydrogenation. Our results demonstrate that the full-surface hydrogenation leads to an expansion in lattice and the $Re_4$ tetramer-chains in the monolayer $ReS_2$ are separated into two dimers in the hydrogenated monolayer. It is calculated that the dynamically stable monolayer of $ReS_2H_2$ has 26 Raman-active vibrational modes. Constant volume specific heat calculations are also performed and the results indicate that at high temperature, the monolayer $ReS_2$ approaches to limit of 3R before the monolayer $ReS_2H_2$. By performing the electronic band structure calculations, it is shown that when the $ReS_2$ surface is fully hydrogenated, there occurs a direct to indirect band gap transition and the semiconducting hydrogen-induced monolayer has a band gap of 0.74 eV.

**Keywords:** Rhenium Disulfide, Hydrogenation, Surface functionalization, Electronic properties, Vibrational properties

## 1. INTRODUCTION

After the discovery of graphene [1], research on novel two-dimensional (2D) materials, such as transition metal dichalcogenides (TMDs) (*e.g.*, $MoS_2$ [2], $MoSe_2$ [3] and $WSe_2$ [4]), has grown rapidly. Since bulk counterparts of these materials are composed of atomically thin single layers bonding via weak van der Waals forces, it is relatively easy to access to large-area 2D forms with the high structural quality [5]. 2D TMD type materials exhibit unique properties such as mechanical flexibility [6-7], electronic and optical attributes [7-10] with comparing to their bulk counterparts, as well as most of them possess isotropic behavior [11].

Recently, as new members, semiconducting monolayers of rhenium dichalcogenides ($ReS_2$ and $ReSe_2$) [12] joined to TMD family. Monolayers of $ReS_2$ and $ReSe_2$ show anisotropic electronic and optical properties [13] owing to their distorted 1T phase and the thickness dependency of their band gaps is relatively weaker [14] than the other TMDs. The studies on $ReS_2$ and $ReSe_2$ reveal that it is possible to manipulate the magnetic, electronic and optical properties of such materials by doping [15], formation of lattice defects [16], and applied strain [17]. Moreover, surface functionalization is an useful technique to achieve tuning and controlling the physical properties of the materials [18]. For instance, it was recently reported that the monolayer $ReS_2$ undergoes a phase transition and turns into an indirect-gap semiconductor when the monolayer is fully hydrogenated [19].

In this study, vibrational, electronic and thermal properties of fully hydrogenated $ReS_2$ ($ReS_2H_2$) are investigated by means of first-principles calculations. The monolayer of $ReS_2H_2$ is calculated to be dynamically stable and it is found that the full-surface hydrogenation leads to a direct to indirect band gap transition and also a decrease in the value of the band gap. Moreover, Raman activities of the

*Corresponding Author: hasansahin@iyte.edu.tr
Received: 05.04.2018 Accepted: 27.09.2018

vibrational modes are analyzed. Entropy and constant volume specific heat values of the monolayer $ReS_2H_2$ are found to be lower than that of the monolayer $ReS_2$.

## 2. COMPUTATIONAL DETAILS

We performed the first-principles calculations based on density functional theory (DFT) employing the plane-wave basis projector augmented wave (PAW) method as implemented in the Vienna *ab*-initio Simulation Package (VASP) [20-21]. The generalized gradient approximation (GGA) was adopted for the exchange-correlation potential as parameterized by Perdew-Burke-Ernzerhof (PBE) functional [22]. The DFT-D2 method of Grimme [23] was used to describe the van der Waals (vdW) interactions. Bader technique [24] was used in order to analyze the charge transfer in the structures.

The electronic and geometric relaxations were performed by using Gaussian smearing with broadening of 0.05 eV and the plane wave basis set with the energy cut-off value of 500 eV. The convergence threshold for the total energy minimization was taken to be $10^{-5}$ eV and $10^{-4}$ eV/Å for the energy difference between each consecutive electronic step and Hellmann-Feynman forces on each unit cell, respectively. The structures were relaxed until the pressure on each unit cell was reduced below 1 kbar in all three directions. A vacuum space of 18 Å was applied in perpendicular direction to prevent interactions between the adjacent layers. Γ-centered 15×15×1 k-point mesh was used for the Brillouin Zone (BZ) integration of the conventional unit cells. The spin-orbit coupling (SOC) was taken into consideration for the band gap estimation.

The phonon dispersions and the thermal properties of the structures were investigated by using the small displacement method as implemented in the PHON code [25]. For the calculations of phonon band diagram and thermodynamic quantities, 2×2×1 and 3×3×1 supercells were considered for $ReS_2$ and $ReS_2H_2$, respectively.

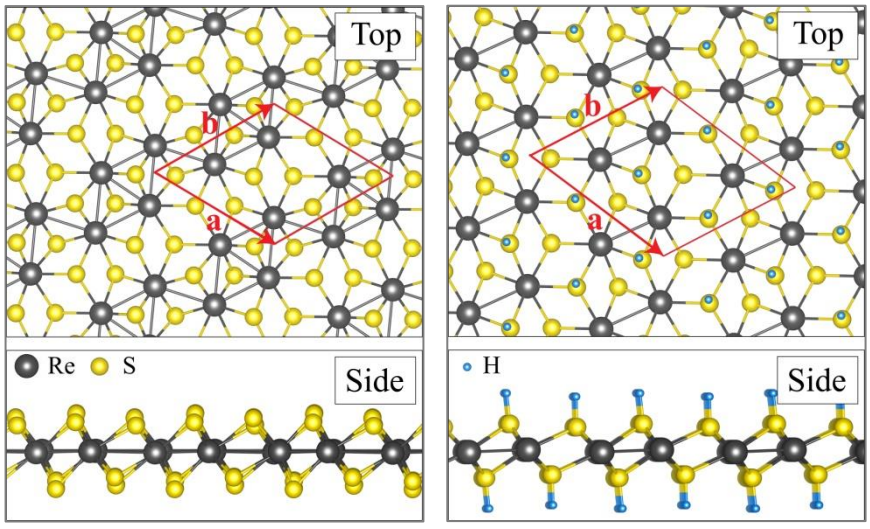


**(a)** **(b)**

**Figure 1.** (Color online) Top and side views are shown for the monolayers of (a) $ReS_2$ and (b) $ReS_2H_2$. Red rhombuses represent the conventional unit cells.

## 3. STRUCTURAL PROPERTIES

Unlike other TMDs, distorted 1T structure with $C_i$ point group symmetry [26] is energetically the most favorable phase for the monolayer $ReS_2$ [27]. As seen in Figure 1 (a), the conventional unit cell of the monolayer $ReS_2$ consists of four Re atoms gathered into a $Re_4$ tetramer-chain surrounded by eight S atoms. The bonds forming the sides of the $Re_4$ tetramer-chain are calculated to be 2.81 Å, while the diagonal Re-Re bond in the tetramer-chain has a length of 2.71 Å. It is calculated that the Re-S bonds are vary between 2.36 and 2.51 Å.

However, it is also seen that full hydrogenation of the surface is possible through one-by-one H atom adsorption on each S atom. The full-surface hydrogenation leads to expansion of the lattice, as a consequence of the expansion; Re atoms are found to be dimerized (see Figure 1 (b)) instead of the tetramer-chains. The Re-Re bond length in a dimer is calculated to be 2.90 Å. The monolayer $ReS_2$ has a thickness of 2.57 Å as seen in Table 1. When the structure is fully hydrogenated, it reaches a thickness of 4.99 Å due to the S-H bonds of length 1.38 Å.

**Table 1.** Calculated parameters for the monolayers of $ReS_2$ and $ReS_2H_2$ are; the lattice constants, a and b; the thickness, t; the average charge donation of Re, $\Delta\rho$; $E_g^{PBE}$ and $E_g^{PBE+SOC}$ the energy gap values calculated within PBE and PBE+SOC, respectively, and $\Phi$, workfunction.

| Structure | a (Å) | b (Å) | t (Å) | Δρ (Å) | $E_g^{PBE}$ (eV) | $E_g^{PBE+SOC}$ (eV) | Φ (eV) |
|---|---|---|---|---|---|---|---|
| $ReS_2$ | 6.46 | 6.38 | 2.57 | 0.9 | 1.47 | 1.34 | 5.54 |
| $ReS_2H_2$ | 7.46 | 6.65 | 4.99 | 0.7 | 0.70 | 0.74 | 3.06 |

In addition, local potentials for the monolayers of $ReS_2$ and $ReS_2H_2$ are demonstrated in the direction of the *z*-axis. As seen in Figure 2, for both of the structures, the lowest potential, as well as the deepest potential well, occurs at the S sub-layers, which indicates that the most of electrons resides at S atoms when a charge transfer to the structure is carried on. It is also seen that S slab of $ReS_2H_2$ is energetically less favorable than that of the $ReS_2$ and the calculated potential energy difference between the Re and S slabs of the monolayer $ReS_2H_2$ (4.60 eV) is slightly lower than that of the $ReS_2$ (4.83 eV) which is resulting from the slight weakening of Re-S bonds. There also occurs a local minimum at -14.94 eV for Re slab in the monolayer $ReS_2$; however, the local minimum becomes shallow for the monolayer $ReS_2H_2$ resulting from the breaking of the bonds between Re atoms in tetramer-chains.

## 4. VIBRATIONAL PROPERTIES

In order to investigate the vibrational properties, first phononic band dispersion of the $ReS_2$ and $ReS_2H_2$ are calculated. The single-layer $ReS_2$ has 36 phonon branches up to a frequency of 450 $cm^{-1}$ as seen in Figure 3 (a). With the full-surface hydrogenation, the number of the phonon branches increases to 60 and there occurs optical modes with frequencies higher than 450 $cm^{-1}$ (see Figure 3 (b)). The vibrational modes with high frequencies, in the range of 500-2400 $cm^{-1}$, are dominated by the motion of H atoms. Since the H atom is much lighter than the Re and S atoms, it is expected to have higher frequency than that of the Re and S atoms.

Moreover, the off-resonant Raman activities of the vibrational modes are investigated. The phonon modes at the Γ point are calculated by using finite-difference method and each atom in the primitive unit cell is displaced 0.01 Å from its equilibrium point. In order to obtain the corresponding Raman activities, the change of macroscopic dielectric tensor is calculated with respect to each vibrational mode. Our calculations reveal that the phonon spectrum of the single-layer of $ReS_2$ includes 18 Raman-active modes, which include out-of-plane ($A_g$-like), in-plane ($E_g$-like) and coupled ($A_g$+$E_g$) vibrational modes. However, the number of Raman-active modes is 26 for fully hydrogenated

structure. 17 branches of Raman-active modes above 500 $cm^{-1}$ are mainly contributed by motions of H atoms while 6 branches between 260 and 500 $cm^{-1}$ mainly come from the motions of S atoms. 3 branches of the Raman-active modes below 230 $cm^{-1}$ basically correspond to Re vibrations.

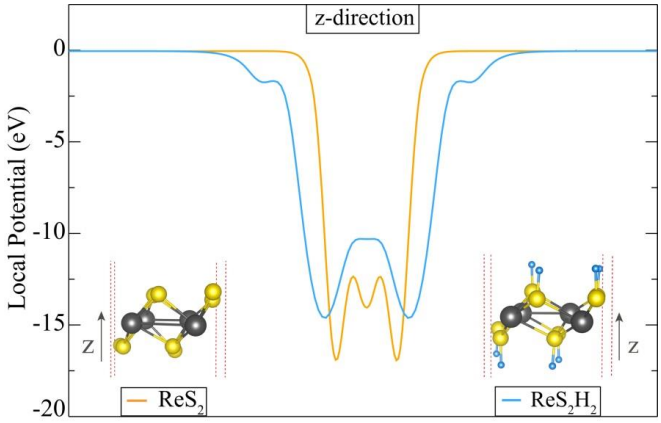


**Figure 2.** (Color online) Local potential profile of monolayers of $ReS_2$ and $ReS_2H_2$ along *z*-axis. Vacuum level is set to zero.

Raman spectroscopy is a useful tool for distinguishing different crystal phases of a material and also for determination of thickness of graphene-like materials. In our calculations Raman tensor, *R*, of a structure is represented by a 3×3 tensor:

$$R=\begin{bmatrix} \frac{\partial \alpha_{11}}{\partial Q_k} & \frac{\partial \alpha_{12}}{\partial Q_k} & \frac{\partial \alpha_{13}}{\partial Q_k} \\ \frac{\partial \alpha_{21}}{\partial Q_k} & \frac{\partial \alpha_{22}}{\partial Q_k} & \frac{\partial \alpha_{23}}{\partial Q_k} \\ \frac{\partial \alpha_{31}}{\partial Q_k} & \frac{\partial \alpha_{32}}{\partial Q_k} & \frac{\partial \alpha_{33}}{\partial Q_k} \end{bmatrix} \quad (1)$$

where the $Q_k$ is the normal mode describing the displacement of each atom in the $k^{th}$ vibrational mode *and* $\alpha_{ij}$ is the polarizability tensor of the crystal structure. Regarding the back scattering experimental geometry, the Raman activity, $R_A$, is represented in terms of Raman invariants which are given by,

$$\beta \equiv \frac{1}{2}\left\{(\tilde{\alpha}_{xx}-\tilde{\alpha}_{zz})^2+(\tilde{\alpha}_{yy}-\tilde{\alpha}_{zz})^2+(\tilde{\alpha}_{zz}-\tilde{\alpha}_{xx})^2+6\left[(\tilde{\alpha}_{xy})^2+(\tilde{\alpha}_{yz})^2+(\tilde{\alpha}_{xz})^2\right]\right\} \quad (3)$$

$$\alpha_s \equiv \frac{1}{3}(\tilde{\alpha}_{xx}+\tilde{\alpha}_{yy}+\tilde{\alpha}_{zz}) \quad (2)$$

where $\alpha_s$ and $\beta$ represent the isotropic and anisotropic parts of the derivative of polarizability tensor, respectively. The $\tilde{\alpha}$ represents the derivative of polarizability with respect to a normal mode. Finally, using these forms of isotropic and anisotropic polarizability derivative tensors, $R_A$, can be written as,

$$R_A = 45{\alpha_s}^2 + 7\beta^2 \quad (4)$$

As seen in Figure 4, the single-layer $ReS_2$ has 3 prominent Raman-active modes more intense than the others and the most intense peak, which has characteristics of mainly the $A_g$-like motion, occurs at 412 $cm^{-1}$. For the hydrogen-induced $ReS_2$, the calculated Raman activities show that the most intense peak located at 2365 $cm^{-1}$ describes the $A_g$-like motion of the H and S atoms. This vibrational mode is relatively more intense than the others; thus, 11 of the 26 Raman-active modes have the intensities closer to zero.

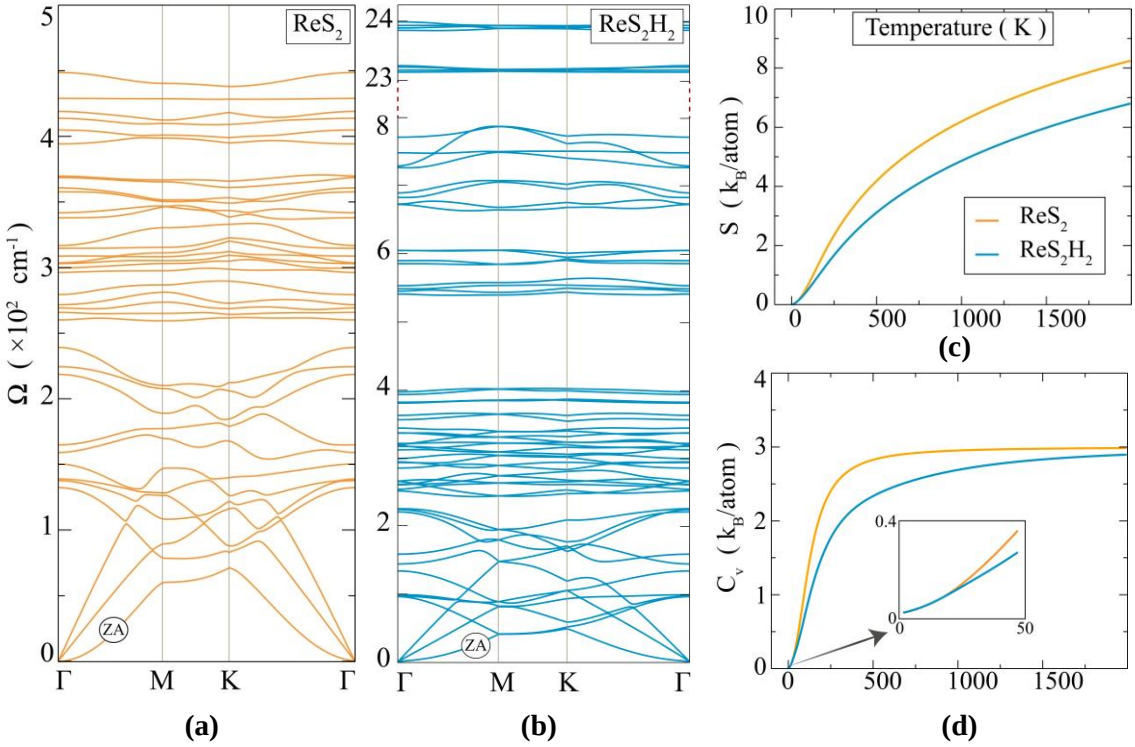


**Figure 3**. (Color online) Phonon band diagrams for the monolayers of (a) $ReS_2$ and (b) $ReS_2H_2$. ZA represents the flexural mode. (c) Entropy and (d) constant-volume specific heat is demonstrated as a function of temperature.

In order to investigate the thermal properties, entropy and specific heat (at constant volume, $C_v$) are calculated for both of the structures (see Figures 3(c) and (d)). It is found that entropy (per atom) and $C_v$ (per atom) of the monolayer $ReS_2$ are larger than that of $ReS_2H_2$. As seen in Figure 3 (d), at high temperature, $ReS_2$ approaches the Dulong-Petit [28] limit before $ReS_2H_2$ which means that the hydrogen-induced structure has a larger Debye temperature than that of $ReS_2$. Moreover, for the 2D crystals, the behavior of the specific heat can be determined by the characteristics of flexural mode (labeled as ZA in Figure 3 (a) and (b)) [29, 30].

In the vicinity of Γ point, it is found that the ZA branch of hydrogen-induced structure has a lower group velocity than that of the monolayer $ReS_2$, which indicates the lower $C_V$.

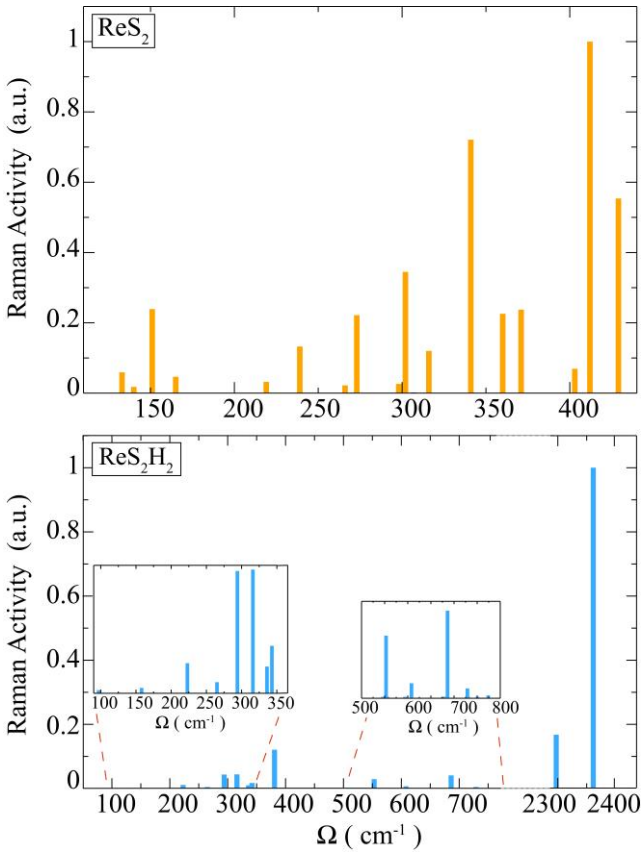


**Figure 4.** (Color online) Relative activities of Raman-active modes are shown for the monolayers of $ReS_2$ (top panel) and (bottom panel) $ReS_2H_2$. In both of the graphs, the highest activities are normalized to 1.

## 5. ELECTRONIC BAND DISPERSION

In this section, the electronic properties of $ReS_2$ and $ReS_2H_2$ are investigated and compared with each other. The monolayer $ReS_2$ contains bonds between transition metal atoms as well as metal-chalcogen bonds, differing from the most of the TMDs. Bader charge analysis shows that Re-S bond has a covalent character and charge donation of Re atom to chalcogen atom is 0.5 *e*. For the monolayer $ReS_2H_2$, H and S atoms are donated 0.1*e* and 0.3*e* charges, respectively. The electronic band structures are calculated within the PBE for the conventional unit cells as mentioned in Sec.2. Since the $ReS_2H_2$ undergoes a structural transition to a new phase that can be represented by a smaller primitive unitcell, the electronic band structure of $ReS_2H_2$ shown in Figure 5 (b) has a folded nature at the zone boundaries. For the band gap estimation, spin-orbit interaction is added to calculations performed with PBE. The spin-orbit interaction changes the band gap values for the both of the structures and decreases the band gap of $ReS_2$ from 1.47 to 1.34 eV and for the monolayer $ReS_2H_2$, slightly increases the band gap value from 0.70 to 0.74 eV. The calculations including spin-orbit interaction reveal that the monolayer $ReS_2$ holds a direct band gap of 1.34 eV. When the monolayer $ReS_2$ is fully hydrogenated, the structure undergoes a direct to indirect band gap transition as seen in Figure 5 and the band gap value decreases to 0.74 eV. Moreover, it is seen that the work function of the monolayers of $ReS_2$ is dramatically reduced from 5.54 to 3.06 eV upon formation $ReS_2H_2$.

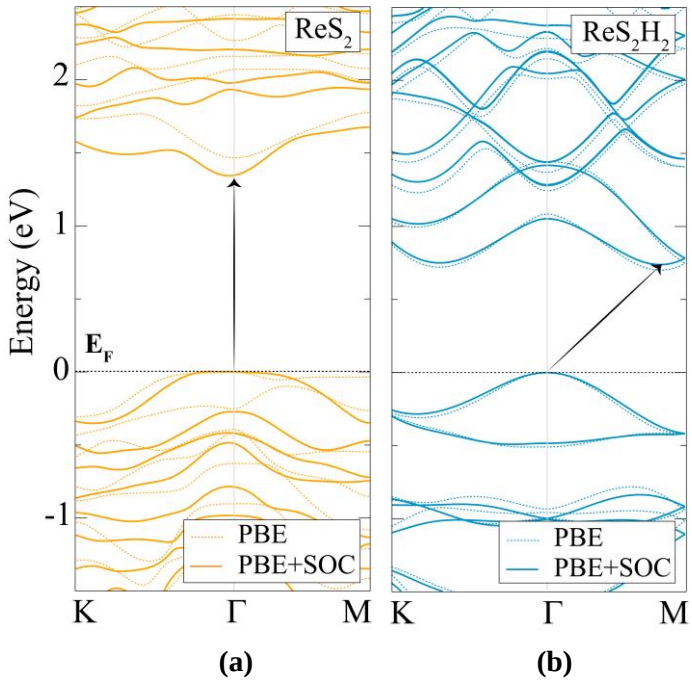


**Figure 5.** (Color online) Electronic band structures are shown for monolayers of (a) $ReS_2$ and (b) $ReS_2H_2$. The Fermi level ($E_F$) is set to zero. The electronic band structure of its conventional unit cell possesses a folded structure since the structural phase of monolayer $ReS_2H_2$ has resemblance to perfect 1T structure.

## 6. CONCLUSIONS

Here, we investigated how the structural, vibrational and electronic properties of the monolayer $ReS_2$ change with the full-surface hydrogenation. The results demonstrated that the hydrogen-induced monolayer, as well as the monolayer $ReS_2$, had a distorted 1T phase in its ground state. However, the hydrogenation leads to lattice expansion and breaking the bonds in the $Re_4$ tetramer-chains. The phonon band calculations showed that the monolayer $ReS_2H_2$ has 60 vibrational modes with frequencies up to 2364.9 $cm^{-1}$, whereas the monolayer $ReS_2$ has frequencies up to 450 $cm^{-1}$. It was found that the modes resulting from the H vibrations are ranging between 500 and 2400 $cm^{-1}$. The Raman-active vibrational modes of hydrogen-induced monolayer were calculated to be 26; however, the Raman-activity of the mode at 2365 $cm^{-1}$ was found to be more intense than the rest of the vibrational modes. In addition, $C_V$ was calculated for both of the structures and the results showed that the Debye temperature increases when the surface of monolayer $ReS_2$ is fully hydrogenated. Calculated electronic band structures revealed that hydrogenation leads to a direct to indirect band gap transition and a decrease in the band gap. Our calculations showed that full-hydrogenation of $ReS_2$ leads to formation of stable $ReS_2H_2$ monolayers that have distinctive electronic and vibrational characteristics.

## ACKNOWLEDGEMENTS

Computational resources were provided by TUBITAK ULAKBIM, High Performance and Grid Computing Center (TR-Grid e-Infrastructure).

## REFERENCES

[1] Novoselov KS, Geim AK, Morozov SV, Jiang D, Zhang Y, Dubonos SV, Grigorieva IV, Firsov AA, Electric field effect in atomically thin carbon films. Science 2004;306: 666-669.

[2] Mak KF, Lee C, Hone J, Shan J, Heinz TF, Atomically thin MoS 2: a new direct-gap semiconductor. Phys. Rev. Lett. 2010; 105: 136805.

[3] Kong D, Wang H, Cha J J, Pasta M, Koski K. J, Yao J, Cui Y, Synthesis of MoS2 and MoSe2 films with vertically aligned layers. Nano Lett. 2013; 13 (3): 1341-1347.

[4] Huang J-K, Pu J, Hsu C-L, Chiu M-H, Juang Z-Y, Chang Y-H, Chang W-H, Iwasa Y, Takenobu T, Li L-J, Large-area synthesis of highly crystalline WSe2 monolayers and device applications. ACS Nano 2014; 8 (1): 923-930.

[5] Magda GZ, Petõ J, Dobrik G, Hwang C, Biró LP, Tapasztó L, Exfoliation of large-area transition metal chalcogenide single layers. Sci. Rep. 2015; 5: 14714.

[6] Castellanos-Gomez A, Poot M, Steele GA, van der Zant HSJ, Agraït N, Rubio-Bollinger G, Elastic properties of freely suspended MoS2 nanosheets. Adv. Mater. 2012; 24: 772-775.

[7] Velusamy DB, Kim RH, Cha S, Huh J, Khazaeinezhad R, Kassani SH, Song G, Cho SM, Cho SH, Hwang I, Lee J, Oh K, Choi H, Park C, Flexible transition metal dichalcogenide nanosheets for band-selective photodetection. Nat. Commun. 2015; 6: 8063.

[8] Wang QH, Kalantar-Zadeh K, Kis A, Coleman JN, Strano MS, Electronic and optoelectronics of two-dimensional transition metal dichalcogenides. Nat. Nanotech. 2012; 7: 699-712.

[9] Chhowalla M, Shin HS, Eda G, Li L-J, Loh KP, Zhang H, The chemistry of two-dimensional layered transition metal dichalcogenide nanosheets. Nat. Chem. 2013; 5: 263-275.

[10] Podzorov V, Gershenson ME, Kloc Ch, Zeis R, Bucher E, High-mobility field-eefect transistors based on transition metal dichalcogenides. Appl. Phys. Lett. 2004; 84: 3301.

[11] Liu E, Fu Y, Wang Y, Feng Y, Liu H, Wan X, Zhou W, Wang B, Shao L, Ho C-H, Huang Y-S, Cao Z, Wang L, Li A, Zeng J, Song F, Wang X, Shi Y, Yuan H, Hwang H. Y, Cui Y, Miao F, Xing D, Integrated digital inverters based on two-dimensional anisotropic ReS2 field-effect transistors. Nat. Commun. 2015;6, 6991.

[12] Tongay S, Sahin H, Ko C, Luce A, Fan W, Liu K, Zhou J, Huang YS, Ho CH, Yan JY, Ogletree DF, Aloni S, Ji J, Li SS, Li JB, Peeters FM, Wu JQ, Monolayer behavior in bulk ReS2 due to electronic and vibrational coupling. Nat. Commun. 2014; 5: 3252.

[13] Hafeez M, Gan L, Li H, Ma Y, Zhai T, Large-area bilayer ReS2 film/multilayer ReS2 flakes synthesized by chemical vapor deposition for high performance photodetectors. Adv. Mater. 2016; 26: 4551-4560.

[14] Jariwala B, Voiry D, Jindal A, Chalke BA, Bapat R, Thamizhavel A, Chhowalla M, Deshmukh M, Bhattacharya A, Sythesis and characterization of ReS2 and ReSe2 layered chalcogenide single crystals. Chem. Mater. 2016; 28: 3352-3359.

[15] Cakir D, Sahin H, Peeters FM, Doping of rhenium disulfide monolayers: a systematic first principles study. Phys. Chem. Chem. Phys. 2014; 16: 16771-16779.

[16] Horzum S, Cakir D, Suh J, Tongay S, Huang Y-S, Ho C-H, Wu J, Sahin H, Peeters FM, Formation and stability of point defects in monolayer rhenium disulfide. Phys. Rev. B 2014; 89: 155433.

[17] Yang S, Wang C, Sahin H, Chen H, Li Y, Li S-S, Suslu A, Peeters, FM, Liu Q, Li J, Tongay S, Tuning the optical, magnetic, and electrical properties of ReSe2 by nanoscale strain engineering. Nano Lett. 2015;15: 1660-1666.

[18] Stepanova M, Dew S. (eds.), Nanofabrication, (Springer, Wien, 2012), p. 163.

[19] Yagmurcukardes M, Bacaksiz C, Senger RT, Sahin H, Hydrogen-induced structural transition in single layer ReS2. 2D Mater. 2017; 4 (3): 035013.

[20] Kresse G, Hafner J, Ab initio molecular dynamics for liquid metals. Phys. Rev. B 1993; 47: 558.

[21] Kresse G, Hafner J, Ab initio molecular-dynamics simulation of the liquid-metal-amorphhous-semiconductor transition in germanium. Phys. Rev. B 1994; 49: 14251.

[22] Perdew JP, Burke K, Ernzerhof M, Generalized gradient approximation made simple. Phys. Rev. Lett. 1996; 77: 3865.

[23] Grimme SJ, Semiemprical GGA-type density functional constructed with a long-range dispersion correction. Comput. Chem. 2006; 27: 1787-1799.

[24] Henkelman G, Arnaldsson A, Jonsson H, A fast and robust algorithm for Bader decomposition of charge density. Comp. Mater. Sci. 2006; 36: 354-360.

[25] Alfe D, PHON: a program to calculate phonons using small displacement method. Comput. Phys. Commun. 2009; 180: 2622-2633.

[26] Hart L, Dale S, Hoye S, Webb JL, Wolverson D, Rhenium dichalcogenides: layered semiconductors with two vertical orientations. Nano Lett. 2016; 16(2): 1381-1386.

[27] Yang S, Tongay S, Li Y, Yue Q, Xia J-B, Li S-S, Li J, Wei S-H, Layer-dependent electrical and optoelectronic responses of ReSe2 nanosheet transistors. Nanoscale 2014; 6: 7226-7231.

[28] Petit A-T, Dulong P-L, Study on the measurement of specific heat of solids. Ann. Chim. Phys. 1819; 10: 395.

[29] Balandin AA, Thermal properties of graphene and nanostructured carbon materials. Nat. Mater. 2011; 10: 569-581.

[30] Sahin H, Structural and phononic characteristics of nitrogenated holey graphene. Phys. Rev. B 2015; 92: 085421.